Korean J. Chem. Eng., 40(7), 1760-1766 (2023)
DOI: 10.1007/s11814-023-1401-7

pISSN: 0256-1115
eISSN: 1975-7220

Crystal engineering of quercetin via combined adsorption of polyvinylpyrrolidone and tannin

Jeongeun Kim*, O-Pil Kwon, and Jonghwi Lee*,†**

*Department of Chemical Engineering and Materials Science, Chung-Ang University, Seoul 06974, Korea
**Department of Molecular Science and Technology, Ajou University, Suwon 16499, Korea
(*Received 12 November 2022 • Revised 15 February 2023 • Accepted 21 February 2023*)

Abstract−In nature, the structures and properties of biominerals are frequently precisely and synergistically controlled by two types of additives. However, the combination of two different types of additives has not often been thoroughly examined in the context of chemical, pharmaceutical, and biological crystallization. A combination of a polymeric additive, polyvinylpyrrolidone (PVP), and a low-molecular-weight additive, tannin (TA), was employed to explore the potential for crystal engineering with quercetin as an active compound. The nucleation time was significantly decreased by the additives, and the resulting crystals contained significant amounts of PVP and TA. FTIR spectroscopy analysis was used to confirm the specific molecular interaction between quercetin, PVP, and TA, and the results were consistent with the results of broadened peaks of XRPD, which indicated decreased particle size and aspect ratio. The melting point of quercetin was significantly depressed as the heat of fusion decreased. When two or more additives are combined, it is possible to obtain crystals with properties and structures that cannot be obtained by regular crystallization.

Keywords: Crystallization, Quercetin, Polyvinylpyrrolidone, Tannin, Mesocrystal

INTRODUCTION

For decades, additives for crystal engineering have been used in various fundamental research and applications to modify the physical and chemical properties of crystals [1-3]. A common additive is a molecule with a similar chemical structure to a substrate molecule (i.e., "tailor-made" additives), which has been successfully employed for various crystals [4]. However, this approach requires time-consuming synthesis and purification, and even then, it is difficult to predict how the interactions with the substrate molecules will affect the final crystal properties. Therefore, this strategy has mostly depended on empirical methods. Furthermore, the results of crystal engineering are more unexpected when more than two different additives are used. On the other hand, nature has used this method to precisely control the structures and properties of crystals [5,6]. For example, during biomineralization, two types of additives are commonly used: an insoluble structural material and a soluble material [7]. Combining these two materials results in synergistic effects that can be used to control the structures and properties of biominerals [8], for example, double-walled silica nanotubes with monodisperse diameters. Inspired by crystallization in nature, we sought to maximize the efficiency of crystal engineering by simultaneously using a high-molecular-weight and a low-molecular-weight compound.

The mechanism of the crystal nucleation and growth in presence of an additive can be explained using classical nucleation theory, which mainly focuses on the issues related to molecular interactions, interfacial energy, and metastable zone width [9]. On the other hand, non-classical nucleation theory focuses on the structure evolution influenced by the existence of additives [10,11]. Similar to biomineralization, additives of various molecular weights have been utilized to engineer organic crystals. Polymorphic forms have been commonly engineered using additives of low molecular weights with structural similarities and specific functional groups [12]. The selective surface adsorption of certain polymorphs can promote the crystallization of other free surfaces whose tendencies determine the selectivity of additive for a polymorph. Low-molecular-weight additives can also be used to successfully achieve nonlinear optical and photoluminescent properties, as is the case with polyene crystals [13].

The presence of dissolved polymers in the crystallization solutions of organic or inorganic materials often triggers non-classical crystallization, resulting in crystals with unique properties [14]. This polymer-directed crystallization has been rarely investigated for organic material applications. Atorvastatin was crystallized in presence of generally recognized as safe (GRAS) polymers to achieve formulation stability, processability, and bioavailability [1]. The crystals with significant amounts of polyacrylic acid, polyethylene glycol, chitosan, and polyethylene imine exhibited lower melting temperature, decreased heat of fusion, and enhanced stability. A wide range of *in vitro* release behaviors, from sustained to accelerated, has been obtained, but no direct evidence on the composite crystal structures was provided. Matzger et al. reported a series of studies on the role of polymeric heteronucleants [15,16]. Additives, which mimic the structures of active pharmaceutical ingredients, were conjugated to insoluble polymers, and the resulting polymers acted as heteronucleants, retarding the induction time for crystal formation. Before conjugation, the additives inhibited the growth of the crystal. Accord-

†To whom correspondence should be addressed.
E-mail: jong@cau.ac.kr

ing to reports, poly(N-isopropyl acrylamide) and nitrofurantoin interact strongly, changing the crystal morphology of nitrofurantoin from a needle-like form to a dendritic form [17]. The nucleation and growth rates of the nitrofurantoin crystals decreased, but their water solubility increased.

The combination of two or more additives with low and high molecular weights has seldom been reported for the crystallization of organic materials, although the combination could offer new insights into crystal engineering, similar to the examples of nature's biomineralization. In this study, quercetin was crystallized in the presence of polyvinylpyrrolidone (PVP) and tannin (TA), an additive with a low molecular weight. Both additives do not contain any tailor-made structures similar to quercetin, but they were chosen because of their ability to have significant specific interactions with each other. Particularly, TA is known to be able to physically interconnect PVP chains, resulting in hydrogel networks [18]. Quercetin is a well known natural polyphenol widely distributed in fruits, leaves, seeds, and grains, and its catechol and resorcinol groups can molecularly interact with other functional groups [19,20]. It is well-known for its antioxidative, antiviral, antibacterial, hepatoprotective, antithrombotic, and anti-inflammatory properties, and there are numerous basic researches and clinical reports on its efficacy to treat cancer and other diseases. Quercetin crystallization has been engineered using polyethylene glycol, polyethyleneimine, and polyvinyl alcohol [20]. The positively charged polyethyleneimine showed significantly decreased crystallinity and prolonged nucleation time. The crystal engineering of quercetin can improve its bioavailability since it is a rather hydrophobic polyphenol with low water solubility, which can enable its applications as anticancer drug and hair restorer.

EXPERIMENTAL METHODS

1. Materials

Quercetin (2-(3,4-dihydroxyphenyl)-5,7-dihydroxy-4H-1-benzopyran-4-one) and TA (1,2,3,4,6-penta-O-{3,4-dihydroxy-5-[(3,4,5-trihydroxybenzoyl)oxy]benzoyl}-D-glucopyranose) were purchased from Sigma-Aldrich (St. Louis, MO, USA). PVP (Mn 40 kg/mol), was purchased from Alfa Aesar (WardHill, Massachusetts, USA). Dimethyl sulfoxide (DMSO) and distilled (DI) water were purchased from DaeJung (Siheung-si, Gyeonggi-do, Republic of Korea). For the sample name, the first letters Q, P, and T of quercetin, PVP, and TA are capitalized, and the lowercase letter 'm' is added when PVP and TA are used in relatively large amounts.

2. Drowning-out Crystallization

PVP (quercetin : PVP=10 : 5 or 10 : 1 wt. ratio) was dissolved in DMSO while being stirred (300 rpm for 12 h). Quercetin and TA (quercetin : TA=100 : 10 or 100 : 2 wt. ratio) were dissolved in the PVP solution at 30 mg/mL concentration while being stirred (300 rpm for 1 h). Using a syringe pump (10 mL/h, KDS-100, KD Scientific, Holliston, MA, USA), 40 mL of antisolvent (water) was injected into 2 mL of quercetin solution in a 70 mL glass vial while the mixture was being stirred (300 rpm). Quercetin crystals were filtered (0.45 μm pore size, PTFE-H, Hyundai Micro, Seoul, Republic of Korea) and washed with DI water before being dried in an oven (50 °C, 24 h) and stored in a desiccator (30 RH%).

3. Characterization

The morphology of particles was observed using a scanning electron microscope (SEM) (S-3400N, Hitachi, Japan). The crystal sample was mounted on filter paper (PTFE-H), attached to a sample holder with carbon tape, and then coated with Pt. The crystal diameter and aspect ratio of 50 different particles were measured using Image J software. Transmission electron microscopy (TEM) images were acquired (JEM-F200, JEOL, Tokyo, Japan) using samples prepared immediately after the crystallization process by directly dropping them on a copper grid (CF-300-CU, Electron Microscopy Sciences, Hatfield, PA, USA). After the excess liquid was absorbed using filter paper, the samples were dried in a vacuum oven for 24 h.

The particle compositions were calculated from the absorption peaks at 380 nm, which were detected using a UV-vis spectrometer (Jasco V-670, Tokyo, Japan; 100 nm/min). For sample preparation, 2 mg of powder was dissolved in 50 mL of DMSO for 24 h (300 rpm). The average was obtained from three different samples. The particle size was measured using a particle size analyzer (LA-910, HORIBA, Tokyo, Japan) after sonication for 1 min. The solution obtained immediately after crystallization was used, and DI water was used as an extra medium.

X-ray powder diffraction (XRPD) was conducted using a new D8-Advance X-ray diffractometer (Billerica, MA, USA) and a Cu Kα anode at 40 kV and 40 mA (2θ=5°-40°, 2θ/s=0.00132°/s). The full width half maximum (FWHM) was measured at 2θ=12.48° or 27.38° using Origin Software [21-23]. The results of 12.48° were used for the calculation of crystal size since both data sets produced similar results. Differential scanning calorimetry (DSC) was performed using a PerkinElmer DSC 4000 (Waltham, Massachusetts, USA) analyzer at a temperature range of 30-350 °C and a heating rate of 10 °C/min in a nitrogen gas atmosphere (20 mL/min). The sample weight was 7.5 mg. Fourier-Transform Infrared spectroscopy (FT-IR) absorption was obtained using the NICOLET 6700 (Thermo Scientific, Waltham, Massachusetts, USA; 650-1,700 cm^{-1}, 1,000 scans).

RESULTS AND DISCUSSION

1. Composition of Crystals

The crystallization results revealed strong interactions between quercetin, PVP, and TA, possibly as a result of the interactions be-

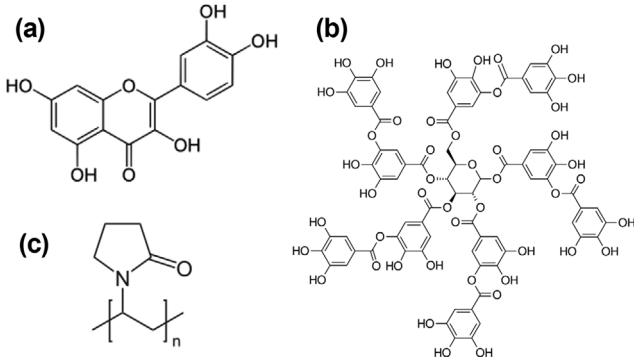

Fig. 1. Chemical structures of (a) quercetin, (b) tannic acid, and (c) polyvinylpyrrolidone.

Table 1. Characteristics of quercetin (Q) samples prepared in presence of PVP and tannic acid (TA)

Designation	Q : PVP : TA (weigh ratio)	Quercetin content (wt%)	Nucleation time (sec)	FWHM
Q	10 : 0 : 0	100	1,033	0.21
QP	10 : 1 : 0	90.2±1	974	0.22
QPm	10 : 5 : 0	85.8±2	920	0.27
QPT	10 : 1 : 0.2	88.5±1	967	0.24
QPTm	10 : 5 : 1	82.7±2	916	0.26

tween hydroxyl, ketone, and pyrrolidone groups (Fig. 1) as hydrogen bonding is possible between the functional groups. It was reported that TA molecules could connect and crosslink PVP chains via hydrogen or ionic bonds [18]. We hypothesize that the physical adsorption of PVP and TA onto crystal surfaces may be caused by the specific interactions of PVP and TA, which could be the main driving factor behind the engineering of quercetin crystals.

The degree of physical adsorption was determined by quantitatively measuring the quercetin content in the obtained crystals. Crystals of 90.2 wt% quercetin and 9.8 wt% PVP were generated from the mother solution of QP, which contained a 9.1 wt% concentration of PVP (Table 1). When the PVP concentration in the mother solution was further increased to 33.3 wt%, 14.2 wt% PVP, which is smaller than 33.3 wt% but still a significant amount, was produced. As previously reported, the content of a polymer is not linearly dependent on the concentration of the polymer in the mother solutions in polymer-directed crystallization [1]. This is due to the low degree of surface adsorption and the limited PVP chain-accessible surface area, which results in a saturation point with full surface coverage. The PVP concentration influenced the particle size, and the surface area available for physical adsorption was unable to keep up with the concentration [24]. A significant PVP content indicates that the obtained crystals had fairly unusual internal structures, such as aggregates of small crystallites with adsorbed PVP chains or crystals with PVP chain defects. The amount of PVP physically adsorbed onto large crystals of micron sizes cannot usually exceed a few wt% [25]. In addition to the surface area of the constituting crystallites, other factors that affect the number of polymer chains in crystals include the strength of physical adsorption, the number of chain adsorption points, etc.

The amount of quercetin was further reduced by the addition of TA (Table 1), lower content in QPT and QPTm than that in QP and QPm. If pairwise additivity was applied, 9.8 wt% PVP (the same as QP) and 1.7 wt% TA would exist in QPT. Complex structures known for TA/PVP in water can form on surfaces or crystal defects [18]. In QPTm, more PVP and TA molecules were available in the solutions, and more molecules were incorporated into the resulting crystals. Therefore, in addition to the interactions between quercetin and PVP, it is possible that the molecular interactions between PVP and TA also contributed to the development of complex structures of quercetin, PVP, and TA. Compared to TA, the relatively large amounts of adsorbed PVP were consistent with the entropy-driven adsorption characteristics of long-chain molecules [26].

Similar trends were found in the nucleation time. With the addition of PVP, a significant decrease in nucleation time was noticed (Table 1). Commonly, macromolecular chains in a solution can solubilize relatively hydrophobic molecules dissolved together, such as quercetin, increasing nucleation time. On the other hand, if macromolecular chains have a steric stabilization effect on the nuclei, the degree of supersaturation required for crystallization will decrease, resulting in a decrease in nucleation time. This stabilization appears to be the case in the current work. The relationship between the quercetin content of solid particles and the nucleation time was not perfectly linear, but generally, the nucleation time decreased as the quercetin content decreased (increase in PVP or TA content). Therefore, the PVP chains can physically adsorb onto the nuclei of quercetin for stabilization, and the nucleation of quercetin crystallization requires a lower supersaturation degree with the addition of PVP. With the extra addition of TA, a lower degree of supersaturation was required for the nucleation. Therefore, the existence of the TA/PVP complex on the surface of the nuclei appeared to be more effective in the stabilization of nuclei than PVP.

2. Crystal Morphology and Size

The presence of PVP and TA induced changes in the crystal habit

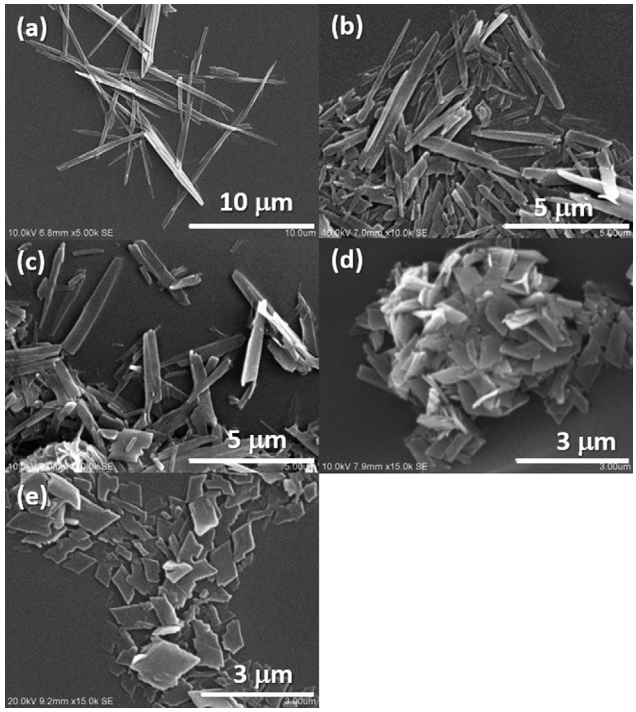

Fig. 2. SEM images of crystals; (a) Q, (b) QP, (c) QPT, (d) QPm, and (e) QPTm.

Table 2. Particle size and aspect ratio values of crystals

Crystals	Particle size from light scattering (μm)	Particle size from SEM images (μm)	Aspect ratio
Q	3.87 (±3.20)	2.31 (±0.43)	20.3 (±6.50)
QP	2.57 (±1.80)	1.58 (±0.38)	8.6 (±3.12)
QPT	3.11 (±1.93)	1.34 (±0.31)	8.4 (±3.21)
QPm	2.99 (±2.35)	1.61 (±0.36)	1.6 (±0.55)
QPTm	2.36 (±1.87)	1.42 (±0.39)	1.6 (±0.58)

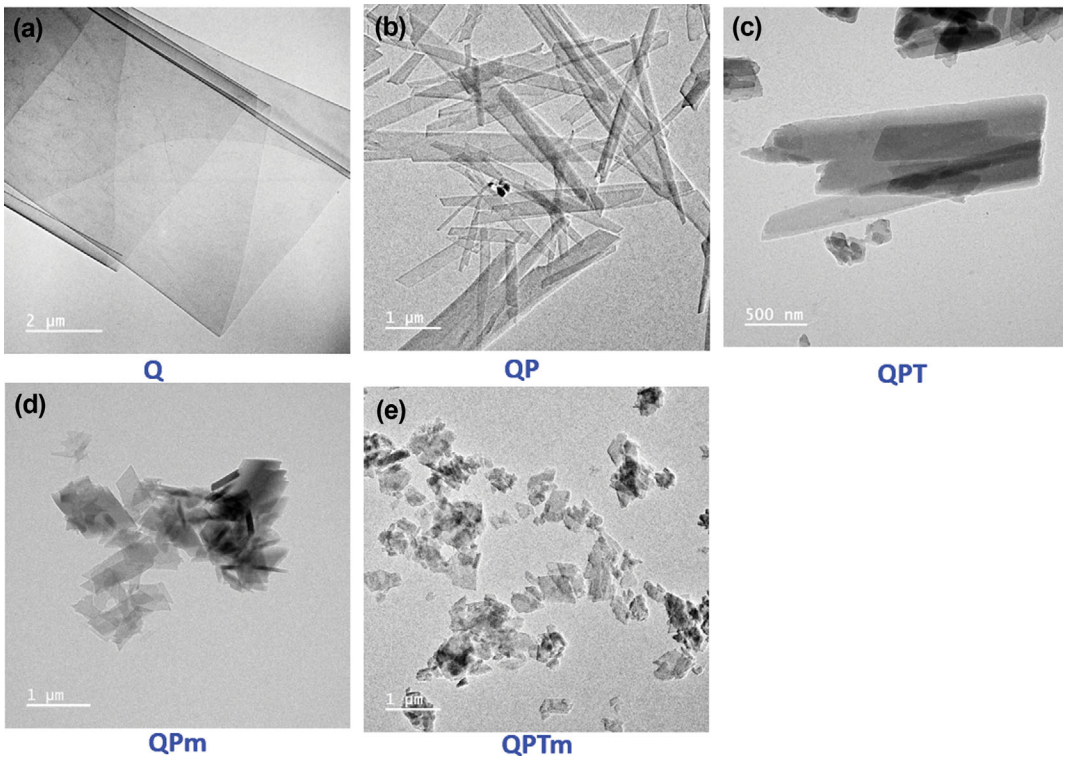

Fig. 3. TEM images of crystals; (a) Q, (b) QP, (c) QPT, (d) QPm, and (e) QPTm.

of quercetin (Fig. 2 and Table 2). The long needle-like morphology of pure quercetin crystals with an aspect ratio of 20.3 was identified in Fig. 2(a). With the addition of PVP, the aspect ratio decreased to 8.6 (QP), and a similar aspect ratio of 8.4 was found in the case of QPT. As the PVP and TA content in the mother liquids increases, the aspect ratio drastically decreased to 1.6 (QPm and QPTm), and the particle morphology had a plate-like morphology (Figs. 2(d) and 2(e)). PVP and TA molecules can adsorb onto the fast-growing surfaces of quercetin crystals, retarding the longitudinal growth of crystals and resulting in a smaller aspect ratio. The diffusion of quercetin molecules onto the growing surfaces of crystals can be hindered by the existence of surface PVP chains and TA molecules.

The particle size decreased as PVP and TA were added, but the trend of the decrease was not as systematic as the aspect ratio. This is probably due to the analysis problems related to the different particle morphologies, i.e., long needles, plates, and significant aggregation [27]. The particle size distribution, as determined by light scattering, ranged up to 10 μm, which was far larger than the size of the particles in Fig. 2 (Fig. S1). Therefore, the major contributors to the particle size distribution are aggregates, not individual crystallites. The SEM images in Fig. 2 show the particle size reduction due to the addition of PVP and TA. The particle size values from the SEM images in Table 2 confirm the results in Fig. 2. The addition of PVP significantly reduced the size of crystals, and the additional incorporation of TA further reduced the size. Interestingly, there were no significant differences between QP and QPm as well as QPT and QPTm. The increase in PVP and TA concentrations did not result in significant particle size reduction. Similar to the trend of crystal composition, the particle size might not be linearly related to the amounts of dissolved PVP and TA.

In Figs. 2(d) and 2(e), QPm and QPTm with low aspect ratios exhibit a sheet-like particle morphology. In Q, QP, and QPT, which have relatively high aspect ratios, it is not clear if the crystal cross-section is rectangular or square (Figs. 2(a)-2(c)). The TEM analysis results confirmed that the cross-section was rectangular, and the crystals were relatively thin (Fig. 3). During TEM analysis, decreases in aspect ratio and particle size as a result of the addition of PVP

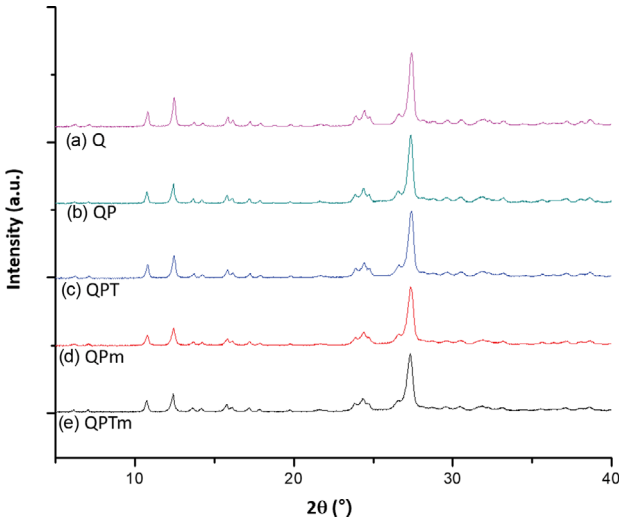

Fig. 4. PXRD patterns of quercetin crystals; (a) Q, (b) QP, (c) QPT, (d) QPm, and (e) QPTm.

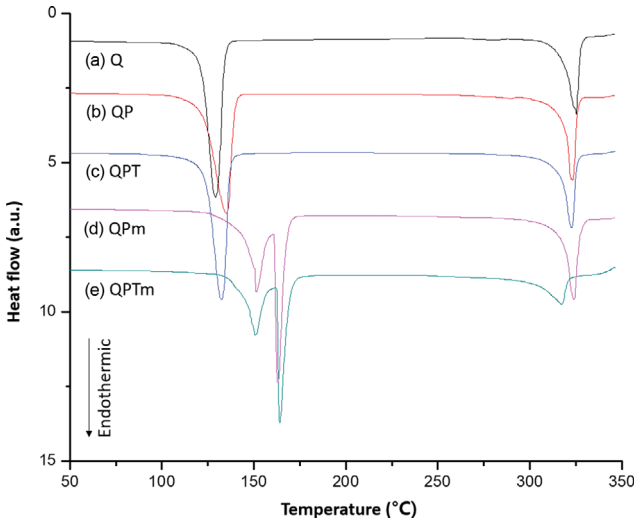

Fig. 5. DSC thermograms of quercetin crystals; (a) Q, (b) QP, (c) QPT, (d) QPm, and (e) QPTm.

and TA were also observed. As the concentrations of PVP and TA increased further, the aspect ratio and particle size decreased. Internal aggregation structures or defects in the crystallite were not identified.

3. Crystal Structure

Although the quercetin content and particle morphology vary widely, the crystal structure of quercetin remained intact. Every sample in Fig. 4 shows the typical XRPD patterns of quercetin, regardless of the inclusion of PVP and TA. Therefore, the presence of PVP and TA did not interfere with the molecular assembly of quercetin to form crystals. Since the size of the crystal phases was altered by the addition of PVP and TA, the broadness of the XRPD peaks may reflect the size variation. Table 1 shows the FWHM results, which indicate the broadening of the XRD peaks, corresponding to the reduction in the size of crystalline phases. The addition of PVP and TA also influenced the defects in the crystal particles, resulting in peak broadening. The Debye Scherrer equation approximated the size of the crystal lattice, which decreased due to the addition of PVP and TA [28].

$$D=K\lambda/\beta\cos\theta$$

where D is the size of the crystal lattice, K is the Scherrer constant (0.9), λ is the wavelength of light used for the diffraction (0.15406 nm Cu Kα), β is the FWHM, and θ is the angle measured. From the equation, it was revealed that the sizes of crystals were 1,360, 150, 260, and 150 nm for QP, QPT, QPm, and QPTm, respectively. Although these sizes do not exactly match the particle sizes in the SEM and TEM images, they distinctly demonstrated a reduction in particle size due to the incorporation of PVP and TA. The values were also inconsistent with those of the size distribution curves obtained from the light scattering measurement (Fig. S1). Owing to the limitations of the formula used, it was considered to be a guessable level of deviation.

The melting transition of quercetin occurred above 300 °C, before which there was an endothermic peak between 120-170 °C, corresponding to the partial quercetin oxidation (Fig. 5 and Table 3). The melting temperature decreased as PVP and TA were added,

Table 3. Thermal characteristics of the melting transition of quercetin crystals

	Q	QP	QPT	QPm	QPTm
Tm (°C)	325.4	323.2	324.0	322.7	317.2
ΔH (J/g)	123.9	119.9	109.8	118.1	72.8

and the increase in the concentrations of PVP and TA further decreased the melting temperature. Similarly, melting enthalpy followed the same trend, indicating decreased crystallinity and decreased size of crystal phases. Particularly, 8.2 °C melting point depression and 41% reduction in enthalpy were found in the case of QPTm. The correlation between melting enthalpy and quercetin content was relatively high, while the relationship between melting temperature and quercetin content was relatively low. The results of melting enthalpy, particle size, aspect ratio, XRPD peak broadening, and nucleation time were all essentially similar because the correlations of particle size, aspect ratio, 1/(FWHM), and nucleation time with quercetin content were generally linear.

Particle size reduction coupled with decreased crystallinity could result in the deterioration of the physical stability of polyphenols. On the other hand, the surface physical adsorption of long-chain molecules can restrict oxidation in quercetin and increase stability. Fig. 5 shows the shifts in oxidation peaks to higher temperatures by the incorporation of PVP and TA. Both QP and QPT exhibited oxidation peaks at higher temperatures. When the content of PVP and TA increased, the oxidation peak was split into two, and both peaks were much higher than that of Q. A comparison between QP and QPT shows that the presence or absence of TA has less effect than that of PVP. QPTm peaks were no different from those of QPm. Therefore, the surface adsorption layer of PVP may act as a protective layer for quercetin, and the presence of TA is unlikely to have a substantial stabilizing or antioxidant effect on quercetin.

Possible molecular interactions were detected in the FT-IR analysis (Fig. 6). The OH bending peak at 1,381 cm^{-1} showed a shift toward a shorter wavelength with the addition of PVP and TA [29].

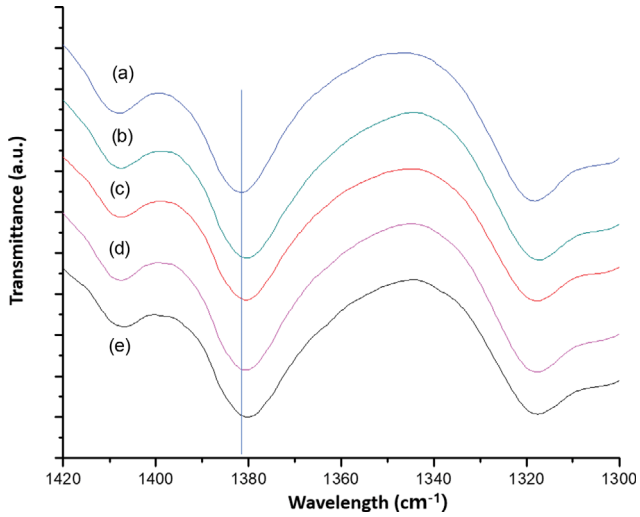

Fig. 6. FT-IR spectroscopy results of -OH bending (1,382 cm^{-1}) and C-H bending (1,318 cm^{-1}) bands; (a) Q, (b) QP, (c) QPm, (d) QPT, and (e) QPTm.

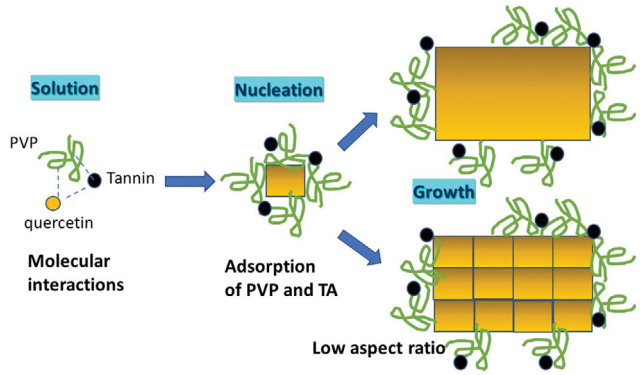

Fig. 7. Tentative crystallization mechanism of quercetin in presence of PVP and tannic acid (TA).

Since PVP does not contain OH, the OH bending peaks of QP and QPm were solely from quercetin, and their shifts resulted from the hydrogen bonding interactions between PVP and quercetin. Therefore, the significant PVP content in the obtained crystals in Table 1 and other correlated results are the results of these interactions. QPT and QPTm showed similar degrees of shift, indicating that the influence of TA might not be as significant as that of PVP. This could be due to the small amounts of TA in the crystals. Similar shifts to shorter wavelengths were also observed in the C=O stretching vibration of 1,664 cm^{-1} and the C=C stretching vibration of 1,562 cm^{-1} and 1,522 cm^{-1} (Figs. S2 and S3). Thus, the specific interactions of C=O and C=C between the molecules can also be expected.

Fig. 7 shows the tentative mechanism of crystal nucleation and growth of quercetin in the presence of PVP and TA. Quercetin molecules exhibited specific molecular interactions with PVP and TA in the solution, and the interactions promoted crystallization while shortening the nucleation time. Upon nucleation of quercetin crystals, the preferential physical adsorption of PVP onto the growing surfaces with or without TA restricted the molecular diffusion of quercetin, reducing the growth rate of the surface [30]. The surfaces with high growth rates were more restricted, and a shorter aspect ratio and reduced particle size resulted as a natural consequence. As a result of the restricted growth, crystals could grow into small crystals (Figs. 2 and 3). Another possibility is that the nanoparticles with adsorbed PVP with or without TA would assemble to form the mesocrystal-like particles shown in Figs. 2 and 3. In any case, PVP and TA could be incorporated into the particles as defects, and this could result in changes in FWHM and the thermal characteristics of quercetin. TA has further effects by enhancing the stability of surface chain anchoring. This crystal engineering, which utilizes the interactions between long and short molecules in a solution, is attractive because it is a convenient strategy for tailoring the physicochemical properties of organic crystals, such as active pharmaceutical ingredients, without altering their crystal structure [31,32].

CONCLUSIONS

The effects of two additives with high and low molecular weights on the crystallization of quercetin, a natural polyphenol, were investigated to develop a new crystal engineering tool. PVP and TA, which are known to interact via hydrogen or ionic bonds, were used as co-solutes in a drowning-out crystallization process. Strong interactions between quercetin, PVP, and TA were confirmed by FT-IR and other characterizations. The nucleation time was shortened by up to 11% owing to the presence of the additives, and significant amounts of PVP and TA more than 10 wt% were incorporated into the resulting crystals. Both particle size and aspect ratio decreased drastically due to the addition of PVP and TA (submicrons from 4 microns and 1.6 from 20.3, respectively), and this was consistent with the results of decreased melting point, decreased heat of fusion, and broadened FWHM. On the other hand, the crystal structure of quercetin molecules was unaffected by the addition of PVP and TA. This combination of two additives with high and low molecular weights could be further engineered by controlling the interactions between the two, and this strategy could offer new crystal engineering insights for future organic material applications.

FUNDING

This study was financially supported by National Research Foundation of Korea (NRF) grants funded by the Ministry of Science and ICT (MSIT) (Engineering Research Center 2021R1A5A6002853) and Ministry of Science and ICT (MSIT) in Korean government and Korea Industrial Technology Association (KOITA) (KOITA-RND3-2-2022-04).

SUPPORTING INFORMATION

Additional information as noted in the text. This information is available via the Internet at http://www.springer.com/chemistry/journal/11814.

REFERENCES

1. H. Choi, H. Lee, M. K. Lee and J. Lee, *J. Pharm. Sci.*, **101**, 2941

(2012).
2. S.-H. Lee, G.-H. Lee, K.-H. Lee, M. Jazbinsek, B. J. Kang, F. Rotermund and O.-P. Kwon, *Cryst. Growth Des.*, **16**, 3555 (2016).
3. Z. X. Ting and L. J. Yan, *Macromol. Res.*, **30**, 325 (2022).
4. R.-Q. Song and H. Cölfen, *Cryst. Eng. Comm.*, **13**, 1249 (2011).
5. E. Kim, S. Agarwal, N. Kim, F. S. Hage, V. Leonardo, A. Gelmi and M. M. Stevens, *ACS Nano*, **13**, 2888 (2019).
6. S. Mann, B. R. Heywood, S. Rajam and J. D. Birchall, *Nature*, **334**, 692 (1988).
7. G. Falini, S. Manara, S. Fermani, N. Roveri, M. Goisis, G. Manganelli and L. Cassar, *Cryst. Eng. Comm.*, **9**, 1162 (2007).
8. E. Pouget, E. Dujardin, A. Cavalier, A. Moreac, C. Valéry, V. Marchi-Artzner, T. Weiss, A. Renault, M. Paternostre and F. Artzner, *Nat. Mater.*, **6**, 434 (2007).
9. S. Xu, D. Cao, Y. Liu and Y. Wang, *Cryst. Growth Des.*, **22**, 2001 (2021).
10. S. Karthika, T. Radhakrishnan and P. Kalaichelvi, *Cryst. Growth Des.*, **16**, 6663 (2016).
11. H. Pyles, S. Zhang, J. J. De Yoreo and D. Baker, *Nature*, **571**, 251 (2019).
12. X. Zhang, J. Wang, F. Yu, X. Cheng, Y. Hao, Y. Liu, X. Huang, T. Wang and H. Hao, *Cryst. Eng. Comm.*, **24**, 854 (2022).
13. O.-P. Kwon, S.-J. Kwon, M. Jazbinsek, A. Choubey, P. A. Losio, V. Gramlich and P. Günter, *Cryst. Ggrowth Des.*, **6**, 2327 (2006).
14. B. Ni, G. Gonzalez-Rubio and H. Cölfen, *Acc. Chem. Res.*, **55**, 1599 (2022).
15. D. S. Frank, Q. Zhu and A. J. Matzger, *Mol. Pharm.*, **16**, 3720 (2019).
16. C. P. Price, A. L. Grzesiak and A. J. Matzger, *J. Am. Chem. Soc.*, **127**, 5512 (2005).
17. T. Munk, S. Baldursdottir, S. Hietala, T. Rades, S. Kapp, M. Nuopponen, K. Kalliomaki, H. Tenhu and J. Rantanen, *Mol. Pharm.*, **9**, 1932 (2012).
18. H. Fan, L. Wang, X. Feng, Y. Bu, D. Wu and Z. Jin, *Macromol. Res.*, **50**, 666 (2017).
19. G. S. Kelly, *Quercetin, Altern. Med. Rev.*, **16**, 172 (2011).
20. H. Kim, J. Kim, O.-P. Kwon and J. Lee, *Macromol. Res.*, **28**, 1276 (2020).
21. C. A. Kadar, M. Faisal, N. Maruthi, N. Raghavendra, B. Prasanna and S. Manohara, *Macromol. Res.*, **30**, 638 (2022).
22. K. Ibtehaj, M. H. H. Jumali, S. Al-Bati, P. C. Ooi, B. A. Al-Asbahi and A. A. A. Ahmed, *Macromol. Res.*, **30**, 172 (2022).
23. S. Kang, H. Kwon, J. Jeong, Y.-C. Kim and J. Park, *Macromol. Res.*, **30**, 454 (2022).
24. C. J. Schram, S. P. Beaudoin and L. S. Taylor, *Langmuir*, **31**, 171 (2015).
25. E. Bouchaud and M. Daoud, *Journal de Physique*, **48**, 1991 (1987).
26. P. Somasundaran and L. Huang, *Adv. Colloid Interface Sci.*, **88**, 179 (2000).
27. P. Hamilton, D. Littlejohn, A. Nordon, J. Sefcik and P. Slavin, *Analyst*, **137**, 118 (2012).
28. U. Holzwarth and N. Gibson, *Nat. Nanotechnol.*, **6**, 534 (2011).
29. W.-H. Chang, P.-Y. Liu, D.-E. Lin, Y.-T. Jiang, C.-J. Lu and Y.-H. H. Hsu, *Macromol. Res.*, **30**, 6 (2022).
30. S. Mehmood, H. Yu, L. Wang, M. A. Uddin, B. U. Amin, F. Haq, S. Fahad and M. Haroon, *Macromol. Res.*, **30**, 623 (2022).
31. H. J. Kim, K. H. Kim, Y. S. Han, Y.-J. Kim and H. M. Lee, *Macromol. Res.*, **28**, 1276 (2022).
32. Y. H. Lee, S. Y. Park, Y. J. Hwang and J. K. Park, *Macromol. Res.*, **30**, 90 (2022).

Supporting Information

Crystal engineering of quercetin via combined adsorption of polyvinylpyrrolidone and tannin

Jeongeun Kim*, O-Pil Kwon, and Jonghwi Lee*,†**

*Department of Chemical Engineering and Materials Science, Chung-Ang University, Seoul 06974, Korea
**Department of Molecular Science and Technology, Ajou University, Suwon 16499, Korea
(*Received 12 November 2022 • Revised 15 February 2023 • Accepted 21 February 2023*)

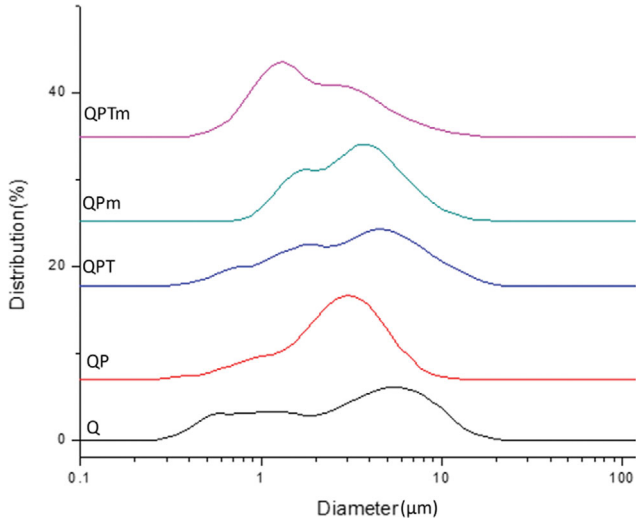

Fig. S1. Particle size distributions of quercetin crystals from light scattering measurement.

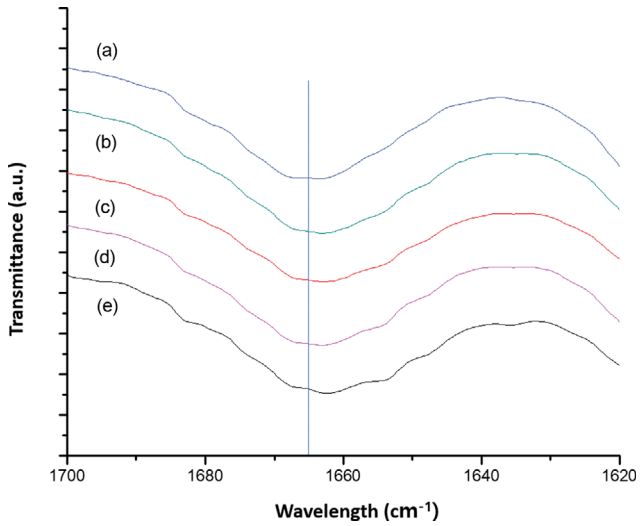

Fig. S2. FT-IR spectroscopy results of C=O stretching bands; (a) Q, (b) QP, (c) QPm, (d) QPT, and (e) QPTm.

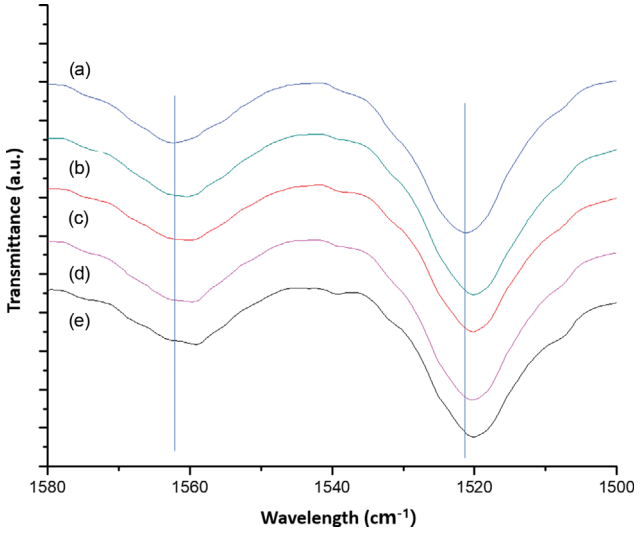

Fig. S3. FT-IR spectroscopy results of aromatic C=C stretching bands; (a) Q, (b) QP, (c) QPm, (d) QPT, and (e) QPTm.